Bonding Geometry and Reactivity of Methoxy and Ethoxy Groups Adsorbed on Powdered TiO_2

Wen-Chun Wu, Chih-Chung Chuang, and Jong-Liang Lin*

Department of Chemistry, National Cheng Kung University, Tainan, Taiwan 701, Republic of China

Received: May 8, 2000

Thermo- and photoreactivities of methoxy ($CH_3O(a)$) and ethoxy groups ($C_2H_5O(a)$) bonded, via the oxygen atom, to one Ti ion (monodentate adsorption form) or to two Ti ions (bidentate adsorption form) on TiO_2 have been studied by Fourier transformed infrared spectroscopy. Regardless of the similar thermal stability for the two adsorption geometries of the adsorbed alkoxy groups, difference in photoreactivity is observed by monitoring the change of their integrated IR absorptions as a function of UV irradiation time. The monodentate photooxidation rate is ∼1.5 times that of bidentate for both methoxy and ethoxy groups. $CH_3O(a)$ on TiO_2 is photooxidized to $H_2O(a)$ and $HCOO(a)$ in the presence of O_2. On the other hand, $C_2H_5O(a)$ is photooxidized to $H_2O(a)$, $HCOO(a)$, and $CH_3COO(a)$. A Russell-like mechanism is invoked to explain the formation of the reaction products. Possible reaction steps that control the photoreactivity of the monodentate and bidentate adsorption forms are discussed in terms of this mechanism.

Introduction

The use of TiO_2 as a photocatalyst for the oxidation of organic molecules has attracted much attention recently.[1,2] TiO_2 has economical, chemical, and electronic advantages that make it an excellent candidate for a photocatalyst. TiO_2 is not expensive and is chemically stable. It is a wide band gap semiconductor with a UV absorption partially overlapped with the solar spectrum, therefore making solar energy as excitation source becomes possible. Furthermore, due to its band edge positions, redox reactions of a large number of molecules can be induced photochemically. The photocatalysis can be carried out with TiO_2 suspended in solutions or with TiO_2 in contact with gas molecules. One of the main purposes in the former system is to destroy organic pollutant molecules present in water. Such studies have proved useful in identifying reaction intermediates and products present in the solution or in the gas phase for a wide range of molecules. Owing to the difficulty in applying surface analytical techniques in these suspension systems, the subjects of surface adsorption and adsorbate's bonding geometry and reactivity have hardly been described. However, for the photoreactions catalyzed by TiO_2 in contact with gas reagents, a few surface analytical techniques are applicable in situ to study the reaction processes in these systems. Previously, Hussein et al. have used the solid−gas interaction to study the adsorption of alcohol molecules on powdered TiO_2 by infrared spectroscopy.[3] It is found that alkoxy groups are formed with monodentate and bidentate bonding geometries after dissociative adsorption of alcohol molecules on TiO_2 as shown in Scheme 1; these two adsorption forms can be distinguished by the C−O stretching frequencies between 1000 and 1200 cm^{-1}.[3−6] The monodentate alkoxy groups exhibit the C−O stretching higher than ∼1100 cm^{-1}, in contrast to the bidentate C−O stretching below ∼1100 cm^{-1}. Recently, Bates et al. have performed first-principles static and dynamic calculation to study the adsorption and decomposition of methanol on stoichiometric $TiO_2(110)$ surface.[7] It is shown in this calculation that methanol can dissociate to form $CH_3O(a)$ groups by O−H or C−O bond cleavage. CH_3O from the O−H bond breakage is bonded to a 5-fold Ti ion for a monodentate coordination. If CH_3OH decomposes by C−O bond breakage, the CH_3 group thus formed is bonded to a bridging oxygen on the surface for a bidentate coordination. As a matter of fact, CH_3O groups from O−H bond breakage of CH_3OH can also form a bidentate coordination by bonding at bridging oxygen vacancy defect sites present on the surface.

SCHEME 1

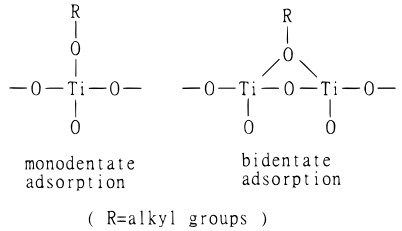

An intriguing question arises regarding the relationship between reactivity and the two bonding geometries of alkoxy groups on TiO_2. In the present study of methoxy and ethoxy groups, we focus on the comparison of thermo- and photoreactivities between monodentate and bidentate forms on powdered TiO_2 by Fourier transformed infrared spectroscopy. The key finding of this work is that the thermal stability shows no surface bonding specificity for monodentate and bidentate adsorption forms, however, monodentate geometry has a larger photooxidation rate than bidentate one for both methoxy and ethoxy groups. To our knowledge, the relation between reactivity and bonding geometry of adsorbates on TiO_2, $CH_3O(a)$ and $C_2H_5O(a)$ in this case, is first demonstrated. A possible mechanism is proposed for the photooxidation of $CH_3O(a)$ and $C_2H_5O(a)$ groups on TiO_2. The difference in the photooxidation reactivity of monodentate and bidentate adsorption forms is discussed in terms of this mechanism.

10.1021/jp0017184 CCC: $19.00
Published on Web 08/18/2000

Experimental Section

The sample preparation of TiO_2 powder supported on a tungsten fine mesh (~6 cm^2) has been described previously.[8,9] In brief, TiO_2 powder (Degussa P25, ~50 m^2/g, anatase 70%, rutile 30%) was dispersed in water/acetone solution to form a uniform mixture which was then sprayed onto a tungsten mesh. After that, the TiO_2 sample was mounted inside the IR cell for simultaneous photochemistry and FTIR spectroscopy. The IR cell with two CaF_2 windows for IR transmittion down to 1000 cm^{-1} was connected to a gas manifold which was pumped by a 60 L/s turbomolecular pump with a base pressure of $\sim 1 \times 10^{-7}$ Torr. The TiO_2 sample in the cell was heated to 450 °C under vacuum for 24 h by resistive heating. The temperature of TiO_2 sample was measured by a K-type thermocouple spot welded on the tungsten mesh. Before each run of the experiment, the TiO_2 sample was heated to 450 °C in a vacuum for 2 h. After the heating, 10 Torr of O_2 was introduced to the cell as the sample was cooled to 70 °C. When the TiO_2 temperature reached 35 °C, the cell was evacuated for gas dosing. O_2 (99.998%) was purchased from Matheson. Methanol (99.8%, BDH) and ethanol (99.8%, Merck) were purified by several cycles of freeze−pump−thaw before introduction to the cell. Pressure was monitored with a Baratron capacitance manometer and an ion gauge. In the photochemistry study, both the UV and IR beams were set 45° to the normal of the TiO_2 sample. The UV light source used was a combination of a 350 W Hg arc lamp (Oriel Corp.), a water filter, and a band-pass filter with a bandwidth of ~100 nm centered at 320 nm (Oriel 51650). The power at the position of TiO_2 sample was ~0.24 W/cm^2 measured in the air by a power meter (Molectron, PM10V1). Infrared spectra were obtained with a 4 cm^{-1} resolution by a Bruker FTIR spectrometer with a MCT detector. The entire optical path was purged with CO_2-free dry air. The spectra presented here have been ratioed against a clean TiO_2 spectrum providing a background reference.

Results

The precedure to prepare methoxy or ethoxy groups on TiO_2 was that a clean TiO_2 surface at 35 °C was exposed to methanol or ethanol vapor followed by evacuation at elevated temperatures. The IR absorptions taken after CH_3OH adsorption and evacuation at 35 °C is shown as the first spectrum in Figure 1a, presenting coadsorption of CH_3OH(a) and CH_3O(a) on the surface.[3,10,11] They are distinguishable by the characteristic symmetric and antisymmetric CH_3 stretching frequencies: 2844 and 2948 cm^{-1} for CH_3OH(a) and 2822 and 2926 cm^{-1} for CH_3O(a). The bands in 1000−1200 cm^{-1} region are due to C−O stretching of the two adsorbed species. After raising the TiO_2 temperature to 200 °C under vacuum, the absorption feature due to CH_3OH(a) is almost removed, as evidenced by the significantly reduced characteristic bands at 2844 and 2948 cm^{-1} shown in Figure 1a, and the surface is basically covered with adsorbed CH_3O(a) groups. The absorption bands due to C−O stretching of CH_3O(a) are peaked at 1045 and 1126 cm^{-1}, reflecting the presence of both bidentate and monodentate forms on the TiO_2 surface.[3−6] The peak area for monodentate 1126 cm^{-1} broad band is ~3 times that for bidentate 1045 cm^{-1} band. Further annealing to 300 °C for 3 min under vacuum, the signal of CH_3O(a) is significantly reduced due to its decomposition on the surface. However, the peak area ratio of 1126 cm^{-1}/1045 cm^{-1} is ~3.3, about the same as that at 200 °C. This result shows, within the experimental error, that mono- and bidentate CH_3O(a) groups have similar thermal stability and suggests that kinetically neither of the two bonding forms is transformed into another during the surface annealing. In the CH_3O(a) photochemistry study, Figure 1b is the IR spectra taken before and after the indicated UV irradiation times during the photooxidation of CH_3O(a) in the presence of O_2. Upon UV irradiation, the baselines of the spectra move upward, especially in the lower frequency region, and the bands in 1000−1200 cm^{-1} range decrease in intensity, showing the consumption of CH_3O(a). Meanwhile, new bands appear at 1362, 1560, and 1619 cm^{-1}. The first two bands are assigned to the −COO− stretching modes of HCOO(a) with bridging coordination; the last band is assigned to adsorbed water molecules.[11,12] In addition, CO_2 (2349 cm^{-1}, not shown) in the gas phase was also found. Note the relative variation of peak area in 1000−1200 cm^{-1} region with UV irradiation in Figure 1b. The peak area for monodentate 1126 cm^{-1} is ~2.9 times of that for bidentate 1045 cm^{-1} before UV irradiation, but this ratio decreases to ~1.2 after a 360 min irradiation. This photooxidation result is different from thermal reaction one and indicates that mono- and bidentate methoxy groups have distinct photoreactivity. In the case of ethanol study, Figure 2 shows the IR spectra of TiO_2 after ethanol adsorption followed by evacuation at the indicated temperatures. For the 35 °C spectrum, absorption bands are peaked at 1049, 1072, 1120, 1264, 1307, 1356, 1379, 1398, 1447, 1473, 1635, 2870, 2931, and 2971 cm^{-1}. The vibrational assignments for the observed frequencies can be divided into four categories in terms of the characteristic absorptions of functional groups: C−O and C−C stretching in 1000−1200 cm^{-1}, O−H bending at 1264 cm^{-1}, CH_2, CH_3 bending in 1280−1500 cm^{-1} and stretching in 2800−3100 cm^{-1}, and H_2O(a) bending at 1635 cm^{-1}. It is found that the absorptions in the 35 °C spectrum are very similar to those observed in the previous IR measurement for TiO_2 following ethanol adsorption studied by Hussein et al.[3] In addition to H_2O(a) present on the surface after ethanol adsorp-

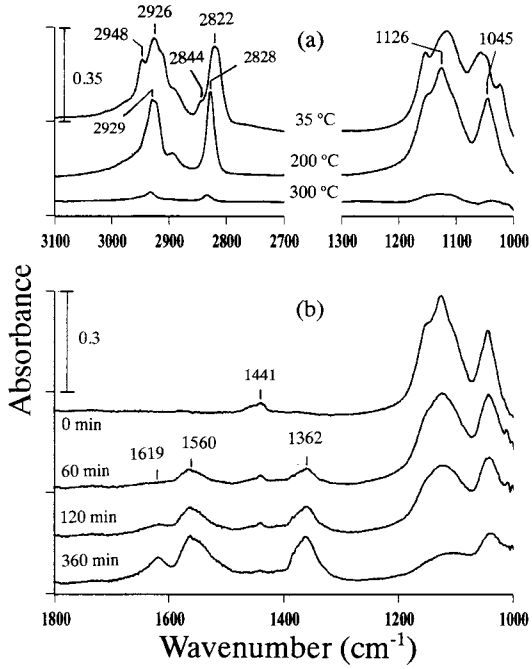

Figure 1. (a) Infrared spectra of a TiO_2 surface exposed to 2 Torr of CH_3OH and then evacuated at 35 °C for 45 min, 200 °C for 1 min, and 300 °C for 3 min. All the spectra were recorded with 100 scans at 35 °C. (b) Infrared spectra taken before and after the indicated UV irradiation times during the photooxidation of CH_3O(a) in the presence of 10 Torr of O_2. The CH_3O(a)/TiO_2 surface was prepared by exposing a clean TiO_2 surface to 2 Torr of CH_3OH followed by evacuation at 220 °C for 1 min. To represent the dynamic behavior, each spectrum was obtained with 5 scans. The TiO_2 used was ~85 mg.

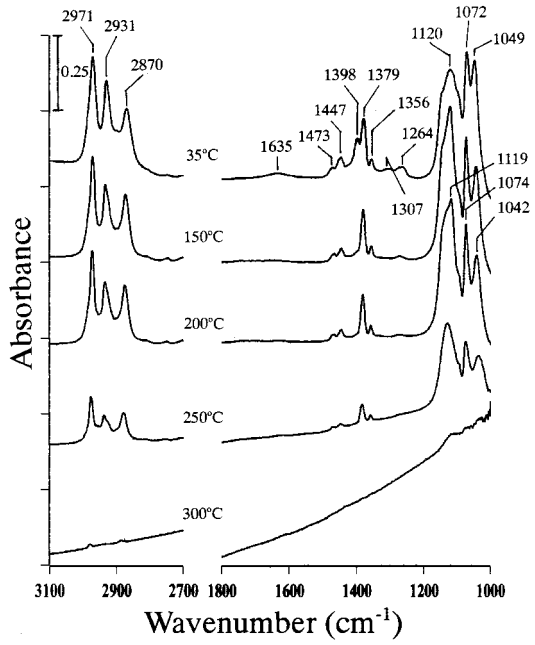

Figure 2. Infrared spectra of a TiO_2 surface exposed to 2 Torr of ethanol and then evacuated at 35, 150, 200, 250, and 300 °C. The vacuation time at 35 °C was 40 min and it was 1 min for the other temperatures. All the spectra were recorded with 100 scans at 35 °C. The TiO_2 used was ~104 mg.

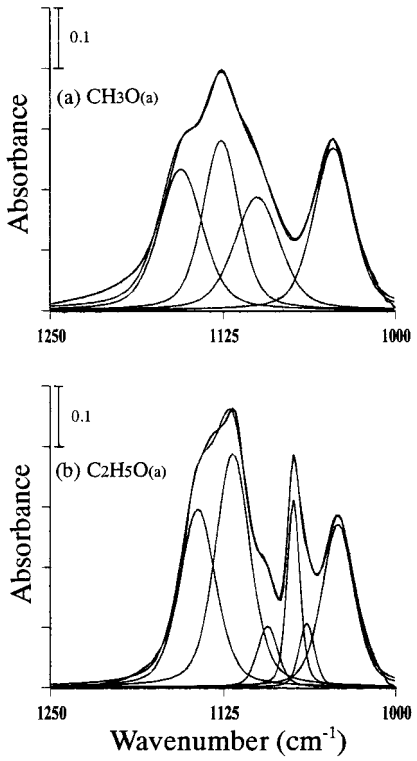

Figure 3. (a) Curve fitting for the spectrum of $CH_3O(a)$ at 200 °C. Each deconvoluted band is made of 40% Lorenz + 60% Gauss. The composed spectrum of the four deconvoluted bands is also shown. The peak positions and widths of the four deconvoluted bands are (1045, 33), (1100, 39), (1126, 31), and (1156, 37). (b) Curve fitting for the spectrum of $C_2H_5O(a)$ at 200 °C. The peak positions and widths for the six deconvoluted bands are (1042, 27), (1064, 13), (1074, 11), (1093, 17), (1118, 29), and (1144, 30).

tion, coadsorbed $C_2H_5O(a)$ and $C_2H_5OH(a)$ are responsible for the infrared bands.[3] The bands of 1264, 1307, and 1398 cm^{-1} are due to O−H bending, CH_2 wagging, and CH_3 symmetric deformation of $C_2H_5OH(a)$, respectively.[3] For $C_2H_5O(a)$, its band frequencies and the corresponding vibrational modes are listed as follows: 1356 cm^{-1} (CH_2 wagging), 1379 cm^{-1} (CH_3 symmetric bending), 1447 cm^{-1} (CH_3 antisymmetric bending), 1473 cm^{-1} (CH_2 scissoring), 2870 cm^{-1} (CH_3 symmetric stretching), 2931 cm^{-1} (CH_2 antisymmetric stretching), and 2971 cm^{-1} (CH_3 antisymmetric stretching). Upon heating to 150 °C, several major changes in the infrared absorptions occur, including variation in the peak shape and relative intensity in 1000−1200 cm^{-1} region and significant drop in intensity for the peaks at 1264, 1307, and 1398 cm^{-1}. These changes are the result of $C_2H_5OH(a)$ desorption and/or decomposition.[3] Meanwhile the $H_2O(a)$ peak at 1635 cm^{-1} is almost completely eliminated. After heating to 200 °C, $C_2H_5OH(a)$ is desorbed or dissociated more thoroughly as indicated by the disappearance of the 1398 cm^{-1} peak. The surface at this temperature is basically covered with $C_2H_5O(a)$ with peak absorptions of C−O and C−C stretching at 1042, 1074, and 1119 cm^{-1}. Higher temperatures cause $C_2H_5O(a)$ decomposition and removal from the surface. Further identification of the C−C and C−O stretching frequencies of $C_2H_5O(a)$ in 1000−1250 cm^{-1} region can be established by referencing the $CH_3O(a)$ absorptions in this range, which only contains C−O stretching, and by decomposing the spectra into deconvoluted bands using a curve-fitting procedure. Figure 3 shows the 200 °C spectra of $CH_3O(a)$ in Figure 1 and $C_2H_5O(a)$ in Figure 2, the deconvoluted bands from optimized spectrum fitting, and their composed spectra. The deconvoluted bands of $CH_3O(a)$ are located at 1045, 1100, 1126, and 1156 cm^{-1} with similar peak widths. The 1045 cm^{-1} belongs to bidentate $CH_3O(a)$ and the last three belong to monodentate one. The deconvoluted bands of $C_2H_5O(a)$ are at 1042, 1064, 1074, 1093, 1118, and 1144 cm^{-1}. Because of the similarity to the $CH_3O(a)$ frequencies, the 1042, 1093, 1118, and 1144 cm^{-1} bands can be assigned to the C−O stretching of $C_2H_5O(a)$; the other bands of 1064 and 1074 cm^{-1} to the C−C stretching. However closely comparing the peak widths, another important indicator in peak assignment, it is found that the 17 cm^{-1} width of the small 1093 cm^{-1} deconvoluted band of $C_2H_5O(a)$ is 22 cm^{-1} less than that of 1100 cm^{-1} of $CH_3O(a)$ and also much smaller than the widths (~28 cm^{-1}) of the C−O stretching at 1042, 1118, and 1144 cm^{-1}; instead, it is close to the widths of the C−C stretching bands at 1064 and 1074 cm^{-1}. Accordingly, the 1093 cm^{-1} is assigned to C−C stretching of $C_2H_5O(a)$ as well. The total peak area for the C−O stretching of monodentate $C_2H_5O(a)$ responsible for the 1118 and 1144 cm^{-1} is ~3 times that of bidentate one responsible for the 1042 cm^{-1} in Figure 3b and this ratio remains approximately the same even as the temperature is raised to 300 °C at which most of $C_2H_5O(a)$ is decomposed and removed from the surface as shown in Figure 2. Monodentate and bidentate $C_2H_5O(a)$ have a similar thermal stability, just as in the case of $CH_3O(a)$. Table 1 lists the absorption frequencies of $CH_3O(a)$ and $C_2H_5O(a)$ observed in the present study and their mode assignments.

Figure 4 is the infrared spectra taken before and after the indicated UV irradiation times during the photooxidation of $C_2H_5O(a)$ in 10 Torr of O_2, showing the decomposition of $C_2H_5O(a)$ and the formation of photooxidation products as demonstrated by the appearance of new bands at 1360, 1381, 1440, 1560, 1621, and 2349 cm^{-1} (not shown). The bands at 2349 and 1621 cm^{-1} are due to gaseous CO_2 and adsorbed H_2O, respectively. The 1360, 1381, and 1560 cm^{-1} bands are due to HCOO(a).[12] The 1440 cm^{-1} band does not belong to the above species. It is already known from Figure 1b that methoxy groups can be photooxidized to HCOO(a). Analogously, in the pho-

TABLE 1: Vibrational Frequencies (cm^{-1}) of $CH_3O_{(a)}$ and $C_2H_5O_{(a)}$ on TiO_2

$CH_3O_{(a)}$		$C_2H_5O_{(a)}$	
1045	ν(C−O) bidentate	1042	ν(C−O) bidentate
1126	ν(C−O) monodentate	1074	ν(C−C)
1441	$\delta_a(CH_3)$	1119	ν(C−O) monodentate
2828	$\nu_s(CH_3)$		
2929	$\nu_a(CH_3)$		
		1356	wag (CH_2)
		1379	$\delta_s(CH_3)$
		1447	$\delta_a(CH_3)$
		1473	sci (CH_2)
		2870	$\nu_s(CH_3)$
		2931	$\nu_a(CH_2)$
		2971	$\nu_a(CH_3)$

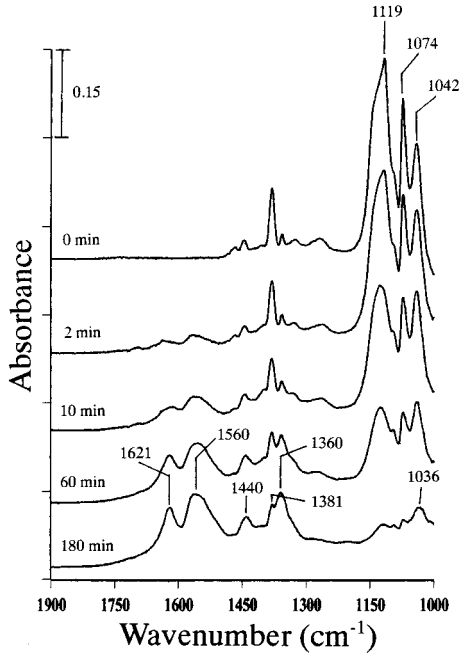

Figure 4. Infrared spectra taken before and after the indicated UV irradiation times during the photooxidation of $C_2H_5O(a)$ in the presence of 10 Torr of O_2. The $C_2H_5O(a)/TiO_2$ surface was prepared by exposing a clean TiO_2 surface to 2 Torr of ethanol followed by evacuation at 185 °C for 3 min. Each spectrum was obtained with 5 scans. The TiO_2 used was ∼73 mg.

tooxidation of ethoxy groups, acetate ($CH_3COO(a)$) is expected to be generated and responsible for the 1440 cm^{-1}. To check this inference, infrared absorptions of TiO_2 following acetic acid adsorption to form acetate was taken. Figure 5a shows the infrared spectra of a TiO_2 surface exposed to 2 Torr of acetic acid and evacuated at 35 and 120 °C. For the 35 °C spectrum, both acetic acid represented by the 1680 cm^{-1} of carbonyl stretching and acetate represented by the 1453 and 1535 cm^{-1} of −COO− symmetric and antisymmetric stretching are present on the surface. Heating to 120 °C under vacuum causes substantial reduction of acetic acid and growth of acetate on the surface. The two major bands for adsorbed acetate in Figure 5 are also observed at similar frequencies in Figure 4 with the −COO− antisymmetric stretching overlapped with that of formate at ∼1550 cm^{-1}, strongly supporting the formation of acetate in the photooxidation of ethoxy groups. The photooxidation of $C_2H_5O(a)$ in the presence of O_2 forms adsorbed acetate, formate, and water. The formate, one-carbon containing species, may originate from photoreaction of the two-carbon containing species of ethoxy and/or acetate. To examine the later possibility,

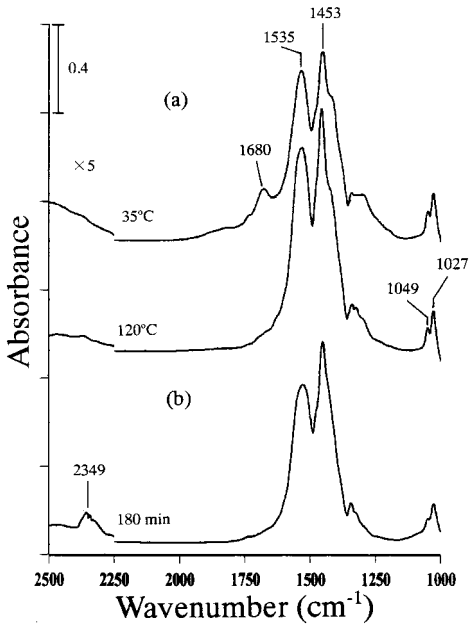

Figure 5. (a) Infrared spectra of a TiO_2 surface exposed to 2 Torr of acetic acid and evacuated at 35 °C for 25 min and 120 °C for 2 min. (b) Infrared spectrum taken after 180-min irradiation during the photooxidation of $CH_3COO(a)$ in 10 Torr of O_2.

photooxidation of adsorbed acetate was carried out. Figure 5b shows the infrared spectrum taken after a 180 min UV exposure during the photooxidation of $CH_3COO(a)$ in 10 Torr of O_2; no $HCOO(a)$ is detected and only CO_2 appear at 2349 cm^{-1}, indicating that the $HCOO(a)$ is due to $C_2H_5O(a)$ photooxidation instead of $CH_3COO(a)$. Note, in the photodegradation of C_2H_5O-(a) in Figure 4, the drop of the peak intensity in 1000−1200 cm^{-1} region is relatively different as evidenced by the bands at 1042 and 1119 cm^{-1} which represent the C−O stretching of bidentate and monodentate forms. Prior to photoirradiation, the total peak area of monodentate C−O stretching (1118 and 1144 cm^{-1}) obtained by curve-fitting is approximately 2.8 times of that of bidentate one (1042 cm^{-1}). However this ratio drops to ∼0.9 after 180-min irradiation. It is noteworthy that the reaction intermediate of $CH_3COO(a)$ formed in ethoxy photoreaction also contains C−C bond: it contributes infrared absorptions at 1027 and 1049 cm^{-1} as shown in Figure 5. It is estimated that for the 180-min spectrum in Figure 4, ∼21% of the bidentate 1036 cm^{-1} peak area is from the contribution of C−C absorption of $CH_3COO(a)$. Taking this into account, the ratio of the peak area of $C_2H_5O(a)$ monodentate C−O stretching to that of bidentate one is still ∼1.1 for the 180 min irradiation spectrum. This result indicates that photoreactivity of $C_2H_5O(a)$ is adsorption-structure dependent, analogous to the case of $CH_3O(a)$ in Figure 1b, and that monodentate form has a higher photoreactivity.

Discussion

Previously, thermal chemistry of methanol and ethanol on TiO_2 has been investigated.[3,13,14] In the case of methanol, it decomposes to generate CH_4, CH_2O, $(CH_3)_2O$, CO, and CO_2. On the other hand, ethanol decomposes to form C_2H_4, C_2H_6, CH_3CHO, $(C_2H_5)_2O$, C_4H_6, and C_4H_8. These products are derived from $CH_3O(a)$ or $C_2H_5O(a)$ chemistry, including dehydrogenation to produce aldehyde, recombination to produce ether, and C−O bond scission to produce alkane and alkene. $CH_3O(a)$ and $C_2H_5O(a)$ are adsorbed on TiO_2 in two adsorption forms of monodentate and bidentate bonding geometries. In the present work, we generate the two bonding forms on TiO_2

SCHEME 2

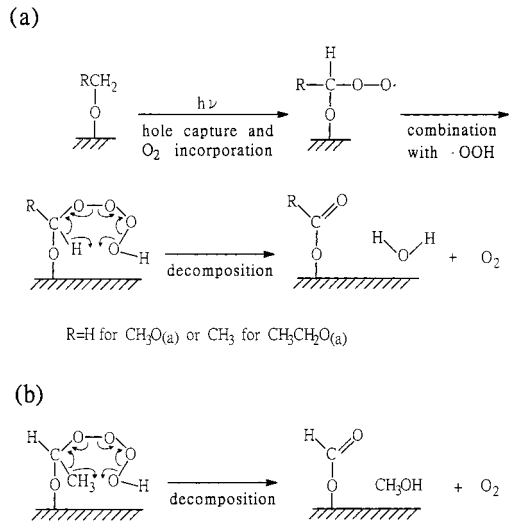

surface and compare their thermal stability by monitoring their integrated infrared absorption changing with surface temperature under vacuum. As shown in Figure 1a, although the total CH_3O-(a) amount may decrease ~70% as the surface temperature is increased from 200 °C to 300 °C, the relative amount of the monodentate form to bidentate one is almost the same, independent with temperature, indicating similar thermal stability for the two bonding geometries. A similar result is observed in Figure 2 in the C_2H_5O(a) case.

In addition to thermal reactions, photochemistry of methanol and ethanol on TiO_2 has been investigated previously.[10,15−20] Methanol can be photooxidized to form CH_2O and $HC(O)OCH_3$; ethanol can be oxided to form CH_3CHO, CH_2O, and HCOOH. Using transient reaction techniques in couple with isotope labeling molecules, Muggli et al. establish a reaction sequence for the photooxidation of a monolayer of ethanol on TiO_2.[17,18] In this sequence, ethanol is first photoconverted to CH_3CHO which undergoes further oxidation and decomposition by two parallel pathways. One pathway is $CH_3CHO \rightarrow CH_3COOH \rightarrow CO_2 + CH_2O \rightarrow HCOOH \rightarrow CO_2$. The other is $CH_3CHO \rightarrow HCOOH + CH_2O \rightarrow HCOOH + CO_2$. Nimlos et al. propose a radical mechanism for the ethanol photooxidation process.[16] In the present work, we study the photochemistry of CH_3O(a) and C_2H_5O(a) on TiO_2 and compare the photooxidation rate for monodentate and bidentate adsorption forms. In the photooxidation of CH_3O(a) in the presence of O_2, surface products of H_2O(a) and HCOO(a) are generated. A Russell-like mechanism, as shown in Scheme 2a using monodentate bonding geometry as an example, has been proposed to explain the formation of H_2O(a) and HCOO(a).[11] At first, CH_3O(a) receives photoholes from TiO_2 band-gap excitation upon UV absorption and in turn dissociates to form $-OCH_2^{\cdot}$ radical and H^+. The formation of $-OCH_2^{\cdot}$ has been reported by Micic et al. in the study of photoreaction of aqueous CH_3O/TiO_2 colloids using ESR technique.[21] The $-OCH_2^{\cdot}$ radical incorporates with O_2 to produce $-OCH_2OO^{\cdot}$ peroxy redicals. UV irradiation on TiO_2 in the presence of oxygen, O_2 can receive photoelectrons to form O_2^- which reacts with H^+ to generate $HOO^{\cdot}$. Finally, $-OCH_2OO^{\cdot}$ and $HOO^{\cdot}$ recombine to form $-OCH_2OOOOH$ tetraoxides, which decompose to HCOO(a) and H_2O(a). The unidentate HCOO(a) shown in Scheme 2a may change to a bridging coordination on the surface. Tetraoxides have been widely investigated and proposed to be reaction intermediates in the radiolysis of aqueous solutions of organic compounds in the presence in O_2.[22] In the photooxidation of C_8 organics with

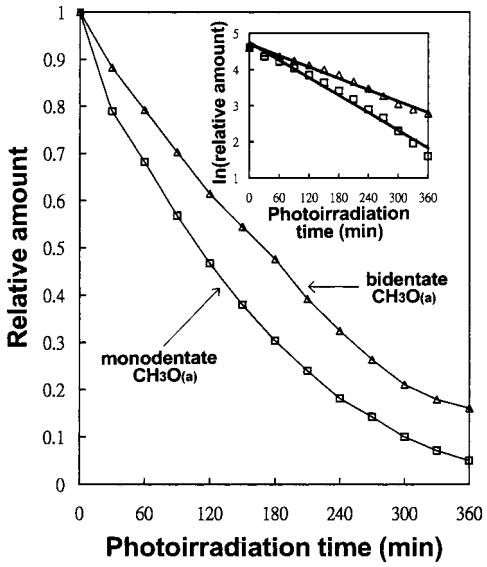

Figure 6. Relative amounts of monodentate and bidentate CH_3O(a) as a function of UV irradiation time. The relative amounts are represented by the total peak areas of monodentate and bidentate C−O stretching obtained by performing curve-fitting procedure. The initial peak areas for the monodentate and bidentate C−O stretching are scaled to 1.

TiO_2-coated glass microbubbles studied by Schwitzgebel et al., organoperoxy and tetraoxide intermediates have been assumed in order to balance the equations of the photocatalytic reactions.[22] On the basis of the correlation between photoinduced charge separation distance and photocatalytic activity in the study of photooxidative degradation of CH_3OH vapor in contact with Pt/TiO_2, Sadeghi et al.[23] have proposed a similar mechanism as Scheme 2a: $CH_3OH + h^+ \rightarrow {}^{\cdot}CH_2OH + H^+$, ${}^{\cdot}CH_2OH + O_2 \rightarrow HOCH_2OO^{\cdot}$, $HOCH_2OO^{\cdot} + {}^{\cdot}OOH \rightarrow HOCHOOOOH \rightarrow HCOOH + O_2 + H_2O$. On the other hand, in the photooxidation of C_2H_5O(a) in the presence of O_2, surface products of H_2O(a), HCOO(a) and CH_3COO(a) are observed. A similar reaction mechanism can explain the formation of H_2O(a) and CH_3COO(a) from C_2H_5O(a) as shown in Scheme 2a. The final step in Scheme 2a is the decomposition of the tetraoxide by the transfer of the hydrogen atom originally bonded to the α-carbon in C_2H_5O(a). If, in the decomposition of the tetraoxide, the group transferred is methyl, instead of hydrogen, as demonstrated in Scheme 2b, the final products are surface HCOO(a) and CH_3OH. The latter can undergo further photooxidation to CH_2O and/or HCOOH and finally to HCOO(a) and CO_2(g). This explains the formation of HCOO(a) together with H_2O(a) and CH_3COO(a) in the present photooxidation of C_2H_5O(a). In the homogeneous phase, migration of hydrogen and alkyl groups have commonly been observed in organic chemistry and organometallic chemistry.[24,25]

Most importantly in the present study, it is found that monodentate adsorption form has a larger photooxidation rate than bidentate one for both CH_3O(a) and C_2H_5O(a). Figure 6 shows the variation of relative monodentate and bidentate CH_3O(a) amounts with UV irradiation time, assuming the surface concentration is proportional to the integrated infrared absorption. In Figure 6, the surface amount of monodentate CH_3O(a) is represented by the sum of peak areas of 1100, 1126, and 1156 cm^{-1} obtained by curve fitting and that of bidentate CH_3O(a) is represented by the peak area of 1045 cm^{-1}. It is found that each the deconvoluted band of 1100, 1126, and 1156 cm^{-1} also follows the same decaying behavior with UV irradiation as their sum. This result is not surprising since they

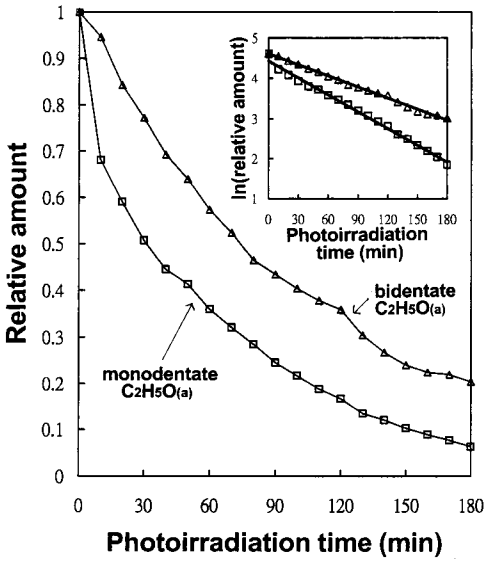

Figure 7. Relative amounts of monodentate and bidentate $C_2H_5O(a)$ as a function of UV irradiation time. The relative amounts are represented by the total peak areas of monodentate and bidentate C−O stretching obtained by performing curve-fitting procedure. The initial peak areas for the monodentate and bidentate C−O stretching are scaled to 1.

are due to the same species of monodentate $CH_3O(a)$. Monodentate $CH_3O(a)$ is depleted more rapidly than bidentate one. The data in the inset of Figure 6 showing ln(relative amount) as a function of irradiation time are fitted with straight lines whose slopes are proportional to rate constants as the assumption of a first-order kinetics for the $CH_3O(a)$ photoconsumption is made. From the slopes, the rate constant for $CH_3O(a)$ monodentate photooxidation is ∼1.5 times of that for bidentate one. Figure 7 is similar to Figure 6, but is for the case of $C_2H_5O(a)$. In Figure 7, the surface amount of monodentate $C_2H_5O(a)$ is represented by the sum of peak areas of 1118 and 1144 cm^{-1} and that of bidentate $C_2H_5O(a)$ is represented by the peak area of 1042 cm^{-1}. The rate constant ratio of monodentate/bidentate $C_2H_5O(a)$ is ∼1.7. It is worthy to note that, although the difference for the rate constants is not very large, it is experimentally detectable and repeatable. One may argue that the change of the C−O stretching peak area for the monodentate absorption relative to the bidentate absorption during photooxidation is due to the change of surface coverage, instead of real difference in photoreactivity, however our thermal studies of $CH_3O(a)$ and $C_2H_5O(a)$ in Figures 1a and 2 have precluded this possibility. In our photooxidation studies, it was noticed that the surface temperatures during the photooxidation of $CH_3O(a)$ and $C_2H_5O(a)$ were increased to ∼ 95 °C; therefore, thermal control experiments were carried out to check the possible thermal effect. In these experiments, the TiO_2 sample with $CH_3O(a)$ or $C_2H_5O(a)$ was held at 95 °C in 10 Torr of O_2 for 360 or 180 min; it showed that the amounts of $CH_3O(a)$ and $C_2H_5O(a)$ were not changed after the surface heating, indicating the decrease of $CH_3O(a)$ and $C_2H_5O(a)$ by UV irradiation was due to photoreaction. Finally, the difference in the photoreactivity of monodentate and bidentate $CH_3O(a)$ or $C_2H_5O(a)$ groups is further described in the framework of the Russell-like mechanism. Examining the reaction pathway in the Russell-like mechanism, the different photooxidation reactivity may originate from electronic effect, which is due to hole capture of $CH_3O(a)$ or $C_2H_5O(a)$ to form $-OCH_2^{\cdot}$ or $-OC_2H_4^{\cdot}$, involving the alkoxy filled states and hole levels generated by TiO_2 photoexitation. Since the monodentate form has a higher photoreaction rate, energetically and spatially more favorable orbital overlap between the two levels involved in the electron transfer is expected to occur for monodentate geometry on the surface.

Conclusion

In the present study, thermal decomposition and photooxidation of $CH_3O(a)$ and $C_2H_5O(a)$ on TiO_2 are studied. These two alkoxy groups have monodentate and bidentate adsorption forms on the surface. It is found that monodentate form has similar thermal stability to bidentate one. However, in the photooxidation in the presence of O_2, the decomposition rate of monodentate form is ∼1.5 times that of the bidentate form. Investigation into the relationship between adsorbate bonding geometry and reactivity is a key issue not only leading to a thorough understanding of elementary reaction processes but also furnishing a knowledge base for improving catalytic reactivity and/or selectivity in practical use.

Acknowledgment. This research was supported by the National Science Council of the Republic of China under Contract NSC-88-2113-M-006-014.

References and Notes

(1) Fox, M. A.; Duley, M. T. *Chem. Rev.* **1993**, *93*, 341.
(2) Hoffmann, M. R.; Martin, S. T.; Choi, W.; Bahnemann, D. W. *Chem. Rev.* **1995**, *95*, 69.
(3) Hussein, G. A. M.; Sheppard, N.; Zaki, M. I.; Fahim, R. B. *J. Chem. Soc., Faraday Trans.* **1991**, *87*, 2655; **1991**, *87*, 2661.
(4) Shchekochikhin, Y. M.; Filimonov, V. N.; Keier, N. P.; Terenin, A. N. *Kinet. Catal.* **1964**, *5*, 94.
(5) Bensitel, M.; Moravek, V.; Lamotte, J.; Sauer, O.; Lavalley J−C. *Spectrochim. Acta, Part A* **1987**, *43*, 1487.
(6) Tsyganenko, A. A.; Filimonov, V. N. *J. Mol. Struct.* **1973**, *19*, 579.
(7) Bates, S. P.; Gillan, M. J. *J. Phys. Chem. B* **1998**, *102*, 2017.
(8) Basu, P.; Ballinger, T. H.; Yates, J. T., Jr. *Rev. Sci. Instrum.* **1988**, *59*, 1321.
(9) Wong, J. C. S.; Linsebigler, A.; Lu, G.; Fan, J.; Yates, J. T., Jr. *J. Phys. Chem.* **1995**, *99*, 335.
(10) Taylor, E. A.; Griffin, G. L. *J. Phys. Chem.* **1988**, *92*, 477.
(11) Chuang, C.-C.; Chen, C.-C.; Lin, J.-L. *J. Phys. Chem.* **1999**, *103*, 2439.
(12) Chuang, C.-C.; Wu, W.-C.; Huang, M.-C.; Huang, I.-C.; Lin, J.-L. *J. Catal.* **1999**, *185*, 423.
(13) Kim, K. S.; Barteau, M. A.; Farneth, W. E. *Langmuir* **1988**, *4*, 533.
(14) Lusvardi, V. S.; Barteau, M. A.; Farneth, W. E. *J. Catal.* **1995**, *153*, 41.
(15) Sauer, M. L.; Ollis, D. F. *J. Catal.* **1996**, *158*, 570.
(16) Nimlos, M. R.; Wolfrum, E. T.; Brewer, M. L.; Fennell, J. A.; Bintner, G. *Environ. Sci. Technol.* **1996**, *30*, 3102.
(17) Muggli, D. S.; Larson, S. A.; Falconer, J. L. *J. Phys. Chem.* **1996**, *100*, 15886.
(18) Muggli, D. S.; McCue, J. T.; Falconer, J. L. *J. Catal.* **1998**, *173*, 470.
(19) Liu, Y. C.; Griffin, G. L.; Chan, S. S.; Wachs, I. E. *J. Catal.* **1985**, *94*, 108.
(20) Carlson, T.; Griffin, G. L. *J. Phys. Chem.* **1986**, *90*, 5896.
(21) Micic, O. I.; Zhang, Y.; Cromack, K. R.; Trifunac, A. D.; Thurnauer, M. C. *J. Phys. Chem.* **1993**, *97*, 13284.
(22) Schwitzgebel, J.; Ekerdt, J.; Gerischer, H.; Heller, A. *J. Phys. Chem.* **1995**, *99*, 5633.
(23) Sadeghi, M.; Liu, W.; Zhang, T. G.; Stavropoulos, P.; Levy, B. *J. Phys. Chem.* **1996**, *100*, 19466.
(24) Morrison, B. T.; Boyd, R. N. *Organic Chemistry*, 3rd ed.; Allyn and Bacon, Inc.: Needham Heights, MA, 1973.
(25) Collman, J. P.; Hegedus, L. S.; Norton, J. R.; Finke, R. G. *Principles and Applications of Organotransition Metal Chemistry*; University Science Books: Mill Valley, CA, 1987.